Design and Performance of the Wedged Pole Hybrid Undulator for the Fritz-Haber-Institut IR FEL

Stephen Gottschalk, Terence DeHart, Robert Kelly, Michael Offenbacker,
Art Valla, John Zumdieck STI Optronics, Bellevue, WA 98004, USA
Sandy Gewinnner, Heinz Junkes, Gerard Meijer, Wieland Schöllkopf,
Weiqing Zhang, FHI, Berlin, Germany,
Hans Bluem, John Rathke, Alan Murray Melville Todd, AES, Medford, NY, USA
Ulf Lehnert, Rossendorf, David Dowell

ABSTRACT

An IR and THz FEL with a design wavelength range from 4 to 500 μm has been commissioned at the Fritz-Haber-Institut (FHI) in Berlin, Germany. Lasing at 28 MeV and a wavelength of 18 μm was achieved in February 2012 [1]. We describe the performance of the undulator built and installed at FHI by STI Optronics for use in the mid-IR range (<50 μm) and 15- to 50-MeV beam energy. The undulator was a high-field-strength wedged-pole hybrid (WPH) with 40-mm period, 2.0-m long, and minimum gap 16.5 mm. A new improvement was including radiation resistance in the magnetic design. We will discuss the measured magnetic and mechanical performance, central and zero steering/offset end-field magnetic designs, key features of the mechanical design and gap adjustment system, genetic shimming algorithms, and control system.

INTRODUCTION

The FHI undulator [1] is shown in Fig. 1. FHI chose a hybrid design because they are more radiation resistant than PPM [6] and wedged poles provide higher field strength. Using NdFeB magnetic material does allow repair of magnets damaged by radiation [3] whereas Sm_2Co_{17} magnetic material must be replaced [13]. Magnet homogeneity data was measured and used for sorting. Tuning used a genetic optimizer [4] to satisfy a number of nonlinear, non-smooth constraints. Mechanics and control systems are based on earlier devices [2]. Performance is summarized in Table 1. Factory acceptance testing was completed in 9 months after start of contract.

RADIATION RESISTANT MAGNETIC DESIGN

Radiation has damaged undulators, [3]. The region damaged operated in the 3rd quadrant. In the 1980s, FEL undulators used $SmCo_5$ magnetic material, then as NdFeB improved and synchrotron radiation rings came online in the 1990's, undulators used NdFeB. Since e-beam emittance is larger on FEL's than storage rings, new facilities like FHI are requesting better radiation resistance. The FHI FEL has some energy collimation from the bend but the undulator is the limiting aperture.

Experiments by Bizen [5,6] confirm that coercivity and permeance ($B/\mu_0 H$) are important. Studies with open circuit magnets (room temperature or cryogenic) do not reflect the more challenging undulator magnetic environment. For example, in [6] the lowest permeance was 0.74 but no part of any undulator magnet operates above a permeance of 0.2. Moderators in front of magnets change the particle and energy spectrum as well as the dose pattern making extrapolation to undulators questionable.

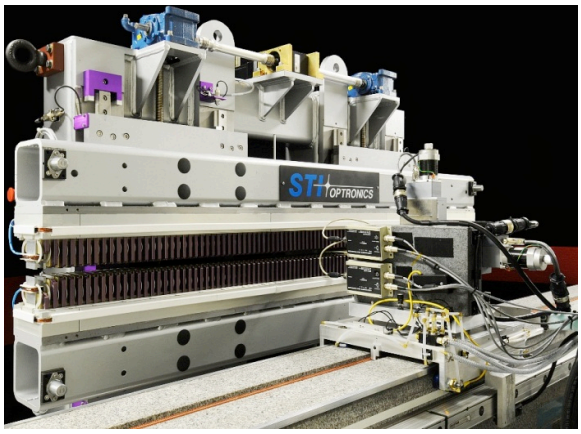

Figure 1: FHI undulator being scanned at minimum gap.

A review of magnet domain theory [9,10] shows that the only mechanism for change of magnetism without melting, baking to Curie temperature or pulverizing magnets is heating above the safe operating temperature for the local permeance. This temperature depends on the anisotropy coefficients for the particular grade and is not directly related to the Curie temperature. When heated, the lowest energy state for the domain becomes a reversed spin orientation [11]. In nucleation magnets like NdFeB, grains enclose domains. Bloch wall energies are sufficiently low that if one domain inside a grain reverses then all domains reverse. Domain sizes range from 5nm to 10 nm and grain sizes are 5-10 μ.

Table 1:

Quantity	**Specification**	**Measured**
Type	Hybrid-Steel or Permendur poles	Hybrid-Permendur poles
Length	2.04 m	2.04 m
Number of periods	50	50
Period	40 mm	40 mm
K_{rms}	1.5 - 0.5	1.62 - 0.5
Peak field at 16.5-mm gap	0.568 T	0.614 T
Gap range	16.5-75 mm	16.5-155 mm
Magnetic material	Sm_2Co_{17} or NdFeB	NdFeB Vacodym 890TP, B_r=1.174T
Beam height	1.2 m ±25 mm 0.1-mm precision	1.2 m±25 mm 0.025-mm precision
Gap resolution	< 1 µm	10-nm linear, 1.85-nm rotary
Gap setting repeatability	0.01mm	<30 nm (using linear encoders)
Gap bi-directional backlash	1 µm	<1 µm
First integral	|I1| < 100 G-cm	13 G-cm at K_{rms}=1.5 -37 G-cm at K_{rms} = 0.5
Second Integral	|I2| < 2600 G-cm^2	1620 G-cm^2 at K_{rms} = 1.5 0 G-cm^2 at K_{rms} = 0.5
Peak-to-peak Trajectory Deviation	-2600 < I2(z) < 2600 G-cm^2	-1300 < I2(z)< 2000 G-cm^2 all gaps
Phase error all gaps	< 5°	4° at K_{rms}=1.5 1.9° at K_{rms} = 0.5
Transverse rolloff at 10mm	< 1% at K_{rms} = 1.5 < 5% at K_{rms} = 0.5	0.7% at K_{rms} = 1.5 1.6% at K_{rms} = 0.5

Radiation heats domains by inelastic collisions [12]. An electron slowing down from 0.5 MeV to 60 keV undergoes about 100,000 collisions with most occurring at low energies. Excitation deposits about 10 eV/collision but ionization can deposit several hundred eV. High-energy electrons have ranges much longer than grain sizes, for example a 1-MeV electron has a range of about 1 mm. As more collisions occur, the scattered electron energy falls below a keV leading to domain heating that can exceed the safe operating temperature.

If the permeance is low, then the magnet will be more sensitive to heating, even if a high coercivity grade is chosen. At zero permeance Sm_2Co_{17} starts losing strength at a temperature of 140 °C while the grade of NdFeB we used operates up to 170 °C [13]. At a 3rd quadrant operating point of $1.25H_{c,B}$[19] the safe temperature is 25 °C lower than the zero permeance value for all grades. Domain permeance decreases during heating because the struck domain is biased in a background field imposed by the surrounding domains, which remain at ambient temperature. It is a small effect for room temperature undulators but potentially large for cryogenic undulators operating below 100 °K, especially because heat capacity, C_p, decreases rapidly with temperature [14].

The approach chosen for this undulator was to use the highest coercivity magnets and operate entirely in the 2nd quadrant. We employed a wedged pole hybrid and permitted quite low permeability, ~60. Safe operating temperature is 170 °C vs. 60 °C for APS U33 [19].

Appropriate codes for detailed Monte-Carlo analyses of domain heating are PENELOPE [7] and Geant4 [8].

Central and End Field Magnetic Design

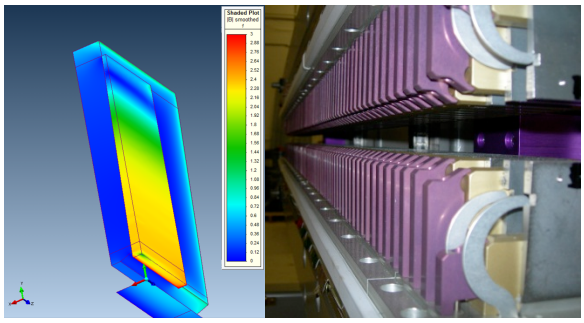

Figure 2: Quarter period FEA and end field for FHI.

The undulator achieves 2nd quadrant operation by aggressive design of magnet and pole shapes near the e-beam. OptiNet was used with a parametric wedged pole model. Initial design used 2D FEA. Next, 3D FEA was used to adjust the magnet overhangs and fine tune the pole height for ease of manufacturing and assembly without changing radiation resistance. The final design is

shown in Fig. 2. Overall, improving radiation resistance reduced field strength 8% relative to APS U33 [19].

The end field design was extended to adjust end magnet and pole heights to explicitly achieve zero entrance offset and angle at multiple gaps. Reducing the height of the 1st and 2nd magnet also protects them from radiation showers if the e-beam hits the 1st pole. Ambient fields were analysed and removed during scanning.

Magnet Homogeneity Mapping

As noted earlier, pole permeability was reduced for radiation resistance. This increased sensitivity to magnet angle errors and homogeneity [15]. A testing method used on early pure permanent magnet undulators (PPM) was to scan $B_y(0,g/2,z)$ [16]. Later, Bahrdt, et al at BESSY [17], moved a magnet past a vertical stretched wire to measure line integrals but the FHI magnets were too large for that device. Horizontal wires sag which compromises accuracy. We used scans of $B_x(x,g/2,z)$ and $B_y(x,g/2,z)$.

The STI scanner was used to acquire sets of 21 transverse scans from x= ± 2cm over a length of 1m. Both B_x and B_y were measured at peak scan speeds of 300mm/sec. Hall probes were Senis YM12 which do not have planar or tensor Hall effects [2]. Scans took 5 minutes/magnet. It ran in parallel with other magnet QA steps so did not add any time to production. The skew to normal multipole correlation plot is shown in Fig. 3 and agrees with open circuit FEA calculations. The few magnets that did not correlate were not used. While our Helmholtz coil has a resolution of 0.01% and correlates with supplier data (R^2>0.9, N>20,000), there was poor correlation (R^2=0.3, N=200) between normal dipoles and Helmholtz vertical angles and R^2 was 0.6 for the skews.

Figure 3: Correlation of skew dipole with normal quadrupole, which matches FEA.

Magnet and Pole Sorting Algorithms

Simulated annealing magnet sorting algorithms use homogeneity scan data as well as Helmholtz strengths. Magnet cost function is a weighted sum 29 factors. Most important were RMS peak fields, half period kicks, I1, I2, dipole, quadrupole, sextupole, rms trajectory error, and rms angle error. Weights are set by device specifications. Pole sorting (virtual shimming) codes include entrance angles and offsets, quadrupoles, internal trajectory, angle deviations and phase errors. Worst case magnet sorting used open circuit models.

KEY FEATURES OF THE MECHANICAL DESIGN AND GAP ADJUSTMENT SYSTEM

Adjustable taper was not a requirement so a single servo motor was used to set the gap. The mechanics are very similar to [2]. Linear encoders were added to set gap in addition to a motor rotary encoder. Their read heads are located as far away from the e-beam as possible.

Tooling balls, scribe lines and optical alignment targets were the same as [2]. The kinematic feet [2] with pitch, roll, yaw, x, y, z adjustments were used.

Three corrector coils were included: entrance and exit one pole "kickers" and a long ambient field corrector. The ambient field corrector is currently off.

Four redundant, 5-nm resolution, Renishaw Resolute BiSS absolute linear encoders measure upstream and downstream half gaps. The servo motor uses a BiSS absolute rotary encoder and drives ballscrews via non-backdriving worm gear boxes. Brakes are not needed. Servos are turned off after the gap is reached.

Bi-directional gap repeatability was independently checked using inboard and outboard digital micrometers. It was <1 μ. Limit switches have certified 2-μ bi-directional hysteresis. Maximum gap opening speed was set to 1 mm/sec.

GENETIC SHIMMING ALGORITHMS

The algorithm and citations to other work are in [4]. The FHI undulator was the first device that we had tuned with this method. Shimming did not need any iteration.

Standard shimming places shims on magnets but for the FHI undulator the radiation resistant design had an unexpected side effect: 3D effects made magnet shims 6X less effective. In fact they would have needed to be so thick that they could change radiation resistance. We adopted pole shims instead [18].

Analyses showed that one 0.001", ten 0.002" and two 0.003" trajectory shims sufficed. Skew quadrupole shims were also added to improve off-axis performance, although this was not a requirement. Measured and wiggle averaged trajectories are shown in Fig. 4. Trajectory deviations decreased as the gap opened. While it is always possible to further improve trajectories, requirements were exceeded so no further adjustments were made.

Figure 4: Trajectory at K_{rms}=1.62.

CONTROL SYSTEM

The rack mounted Ethernet control system is used to change gap, provide status, safety and allow local and remote operation. The system consists of a Galil DMC4040 motion controller, Kollmorgen AKD servo drive for the AKM servo motor. The Galil embedded firmware, safety system, interlocks and GUI are described elsewhere [4]. Each corrector has its own pre-set current vs. gap table burned into the Galil EEPROM, which can be bypassed by EPICS. Corrector supplies are bipolar Kepco BOP models set using 20-bit resolution DAC's inside the Galil controller.

Local control with a laptop was used at STI and prior to EPICS integration at FHI. A multi-tiered, object oriented, VB.NET GUI similar to [4] was used. Source codes for the Galil and VB.NET codes were supplied.

EPICS software was written and tested by FHI. A more detailed discussion can be found in [20].

CONCLUSION

We have summarized the design and performance of a radiation resistant wedged pole hybrid undulator for FHI. All requirements were met.

REFERENCES

[1] W.Schöllkopf et al., "First Lasing of the IR FEL at the Fritz-Haber-Institut Berlin," this conference.

[2] S. Gottschalk, et al, "UCLA Seeded THz FEL Undulator-Buncher Design," this conference.

[3] Sasaki, S, et al, "Radiation Damage to Advanced Photon Source Undulators", Proc. 2005 PAC, Knoxsville, Tenn, p. 4126-4128 (2005).

[4] S. Gottschalk, et al, "The JLAB UV Undulator", this conference.

[5] T. Bizen, et al "High-energy electron irradiation of NdFeB permanent magnets: Dependence of radiation damage on the electron energy" Nucl. Instr. Meth. Phys. Res. 2007 A574, (2007), 401-406.

[6] T. Bizen, et al "Demagnetization of undulator magnets irradiated by high energy electrons", Nucl. Instr. Meth. Phys. Res. A467-468, 2001, 185-189

[7] F. Salvat, et al "PENELOPE-2006:A Code System for Monte Carlo Simulation of Electron and Photon Transport", Workshop Proceedings, Barcelona, Spin, 4-7 July 2006, NEA No. 6222, http://www.oecd-nea.org/science/pubs/2006/nea6222-penelope.pdf.

[8] http://geant4.cern.ch/

[9] A. Hubert, R. Schafer, 'Magnetic Domains: The Analysis of Magnetic Microstructures'. Springer Verlag, Berlin (2000).

[10] K. Buschow, F. DeBoer, 'Physics of Magnetism and Magnetic Materials', Kluwer, NY (2003).

[11] E. Stoner, Wolhlfarth, "A mechanism of magnetic hysteresis in heterogeneous alloys", Phil. Trans. Roy. Soc. A 240, p. 599-644 (1948).

[12] N. Carron, "An Introduction to the Passage of Energetic Particles through Matter", Taylor and Francis, FL (2007).

[13] http://www.vacuumschmelze.com/fileadmin/Medienbiliothek_2010/Downloads/DM/VACODYM_MAX_23MAI12_EN.pdf

[14] H. Fujii, et al, "Heat Capacity and Thermal Expansion of R2Fe14B compounds (R=Y, Nd and Tm)", J. Magnetism and Magnetic Materials 70, p. 331-333 (1987).

[15] K. Robinson, et al, "Hybrid Undulator Design Considerations", Nucl. Instr. Meth. Phys. Res. A250 (1986) 100-109.

[16] Curtin, et al, "A High-Quality Permanent Magnet Wiggler for the Rocketdyne/Stanford Infrared Free Electron Laser", Nucl. Instr. Meth Phys. Res. A272 (1988) 187-191.

[17] J. Bahrdt, et al, "Magnetic Field Optimization of Permanent Magnet Undulators for Arbitrary Polarization", Nucl. Instr. Meth Phys. Res. A516 (2004), 575-585.

[18] S. Gottschalk, et al, "Wiggler Error Reduction through Shim Tuning", Nucl. Instr. Meth. Phys. Res. A296 (1990) 579-587.

[19] S.Gottschalk, et al, "Central Field Design Methods for Hybrid Insertion Devices", Rev. Sci. Instr. 67 (9), September 1996, paper C07 (1996).

[20] H. Junkes, "PAPER"